Fuel 333 (2023) 126362

Contents lists available at ScienceDirect

Fuel

journal homepage: www.elsevier.com/locate/fuel

Full Length Article

Influence of mesoporous iron based nanoparticles on *Chlorella sorokiniana* metabolism during photosynthetic biogas upgrading

Laura Vargas-Estrada [a,b,c], Edwin G. Hoyos [a,b], P.J. Sebastian [c], Raúl Muñoz [a,b,*]

[a] Institute of Sustainable Processes, University of Valladolid, C/Dr. Mergelina s/n., Valladolid 47011, Spain
[b] Department of Chemical Engineering and Environmental Technology, University of Valladolid, C/Dr. Mergelina s/n., Valladolid 47011, Spain
[c] Instituto de Energías Renovables, Universidad Nacional Autónoma de México, Temixco, Morelos CP. 62580, Mexico

ARTICLE INFO

Keywords:
Biogas upgrading
CO_2 biofixation
Iron nanoparticles
Microalgae
UV exposure

ABSTRACT

Three different mesoporous iron based nanoparticles (NPs) were added to *Chlorella sorokiniana* batch cultures devoted to photosynthetic biogas upgrading to enhance CO_2 biofixation: Fe_2O_3, carbon coated zero valent iron NPs containing 7.26 % (wt%) of iron (CALPECH NPs) and carbon coated zero valent iron NPs containing 31.38 % (wt%) of iron (SMALLOPS NPS). The three types of NPs enhanced CO_2 adsorption and therefore biogas upgrading in tests conducted in 1.2 L enclosed photobioreactors. However, the addition of 70 mg L^{-1} of CALPECH NPs resulted in a 2-fold enhancement in the microalgae productivity, and a carbohydrate and lipid content increase by 56 % and 25 %, respectively compared to the control assay. Under UV and visible light irradiation the addition of Fe_2O_3 NPs resulted in a 5.3-times fold enhancement in carbohydrate content when 70 mg L^{-1} was added. Similarly, the addition of 20 mg L^{-1} of SMALLOPS NPs increased the lipid content by 11 % under UV irradiation. Interestingly, CALPECH NPs did not significantly influence *C. sorokiniana* composition, suggesting that these particular NPs can act as UV scavengers. Therefore, the addition of mesoporous nanoparticles could improve CO_2 fixation and microalgae productivity during photosynthetic biogas upgrading.

1. Introduction

Photosynthetic biogas upgrading is based on a solar-driven CO_2 fixation by microalgae that has emerged as an attractive, cost-effective and environment friendly option for CO_2 and H_2S removal from biogas [1–3]. This technology has demonstrated to be feasible in algal-bacterial photobioreactors interconnected to an absorption column [2,4–9], reaching CO_2 removals up to 98.6 % at pilot and demo scale [2,10]. However, there are some challenges and limitations that need to be addressed: i) low CO_2 mass transfer to the culture medium, ii) variations in the liquid and gas flow rates, pH and alkalinity, and iii) diurnal and seasonal variability of environmental parameters influencing photosynthetic activity [11]. Thus, innovative operational strategies are required to enhance CO_2 biofixation during photosynthetic biogas upgrading.

The use of nanoporous materials has recently attracted a renewed attention in the field of CO_2 capture because they exhibit key advantages such as a large surface area to volume ratio, high reactivity, abundant active sites and high adsorption capacity [12]. Metal oxide nanoparticles (NPs) and nanoporous carbons rank among the most popular nanomaterials for CO_2 capture [12]. Three potential mechanisms have been hypothesized to explain the CO_2 capture enhancement by the addition of NPs: 1) bubble breaking effect, where NPs induce a small sized bubble and hence the diffusion area increases; 2) shuttle effect, where the gas is adsorbed to the NPs surface and then is released into the liquid; 3) hydrodynamic effect, where the NPs collide, inducing turbulence and refreshing the liquid–gas boundary layer [13]. The mechanism of interaction will depend on operational factors, such as the type of reactor, agitation and the liquid phase [14]. The shuttle and the hydrodynamic effect have been previously observed in stirred tanks [14,15], although the results reported are contradictory, in both cases the mass transfer was increased. Thus, mesoporous NPs of metal oxides and carbon could represent an innovative tool to enhance CO_2 fixation during photosynthetic biogas upgrading.

The addition of metal oxide NPs to microalgae culture is a controversial topic and the majority of the studies are focused on their toxic effect [16], and the number of studies assessing the benefits of NPs addition on microalgae metabolism is scarce [17]. He et al [17] reported that Fe_2O_3 NPs improved biomass and lipid production up to 39.6 % in *Scenedesmus obliquus* at concentrations < 20 mg L^{-1}. Jeon et al. [18]

* Corresponding author at: Institute of Sustainable Processes, University of Valladolid, C/Dr. Mergelina s/n., Valladolid 47011, Spain.
E-mail address: mutora@iq.uva.es (R. Muñoz).

https://doi.org/10.1016/j.fuel.2022.126362
Received 3 August 2022; Received in revised form 8 October 2022; Accepted 12 October 2022
Available online 20 October 2022

studied the addition of SiO_2 NPs (0.3 % wt) to *C. vulgaris* cultures and observed that NPs enhanced the gas–liquid mass transfer rate of CO_2 by 31 %, and the biomass cell dry weight was increased from 0.48 g L^{-1} (without the NPs) to 1.33 g L^{-1} (with the SiO_2 NPs). The addition of 0.3 g L^{-1} of polymeric nanofibers containing Fe_2O_3 NPs enhanced CO_2 fixation up to 310.9 mg L^{-1} in *Chlorella fusca* LEB 111 cultures [19]. Finally, the addition of 100 mg L^{-1} of graphene quantum dots under UV radiation to *Chlorella pyrenoidosa* cultures enhanced its growth and lipid production by 17 % and 34 % respectively [20]. The effect of NPs has been studied in microalgae growth and macromolecular composition but little information is available in literature on the influence of metal oxide NPs and carbon NPs on photosynthetic biogas upgrading and on microalgae composition.

This work assessed the influence of three types of iron based NPs on *Chlorella sorokiniana* cultures devoted to biogas upgrading: Fe_2O_3 and two different carbon-coated zero-valent NPs. This study investigated the effect of these NPs and the type of irradiation (visible *versus* visible + UV) on CO_2 removal kinetics and on the growth kinetics and composition of *C. sorokiniana*.

2. Materials and methods

2.1. Nanoparticles and stock solutions

Fe_2O_3 NPs were synthesized according to [21]. Carbon coated zero-valent iron (ZVI) (31.38 % of Fe, wt.%) NPs were kindly donated by SMALLOPS and carbon coated ZVI (7.26 % of Fe, wt.%) NPs were kindly donated by CALPECH. The surface area, morphology, pore volume, average pore diameter and elemental composition of the three NPs was determined. Fresh stock solutions of 200 mg L^{-1} of each nanoparticle were prepared in microalgae culture medium and sonicated for one hour to prevent nanoparticle agglomeration in order to facilitate the addition of the NPs.

2.2. Microalgae culture and biogas

The microalgae used in this study was *C. sorokiniana* 211/8k, which was originally purchased from the Culture Centre of Algae and Protozoa (Cambridge, UK). *C. sorokiniana* was stored at 4 °C on sterile agar plates in SK medium enriched with glucose (3.125 g L^{-1}), peptone (0.0625 g L^{-1}) and yeast extract (0.0625 g L^{-1}) according to [22,23]. An inoculum of *C. sorokiniana* was grown at 25 °C in enriched SK medium under continuous illumination (900 μE $m^{-2}s^{-1}$) and shaken at 300 rpm. When the culture reached the exponential growth, the culture was centrifuged (10000 rpm, 4 °C), washed several times and resuspended in distilled water to reach a final concentration of 24 g L^{-1} of total suspended solids (TSS).

To elucidate the effect of nanoparticles on *C. sorokiniana* cultures devoted to biogas upgrading, two different synthetic biogas mixtures were used: Biogas A composed of CO_2 (30 %) and CH_4 (70 %) (Carburos Metalicos; Spain), and Biogas B composed of CO_2 (29.5 %), H_2S (0.5 %) and CH_4 (70 %) (Abello Linde; Spain).

2.3. Experimental set-up

Batch assays were conducted in 1.2 L glass narrow neck bottles to evaluate the effect of the three types of nanoparticles (Fe_2O_3, CALLPECH NPs, SMALLOPS NPs) at different concentrations (0, 20, 40 and 70 mg L^{-1}) and under different light sources (visible *versus* visible + UV) on biogas upgrading by *C. sorokiniana*. The bottles were prepared containing 1 L of the corresponding synthetic biogas in the headspace and 0.2 L of mineral salt medium rich in carbonates as described elsewhere [8] and the corresponding NP concentration. The mineral medium and the corresponding nanoparticle concentration were added to the bottles, which were then closed with butyl septa and plastic caps. The bottles were initially flushed with helium for 5 min and subsequently the corresponding synthetic biogas was flushed for 5 min using inlet and outlet needles to replace the helium headspace. After one hour of stabilization (300 rpm, 25 °C), the bottles were inoculated with *C. sorokiniana* at an initial concentration of 200 mg L^{-1} of TSS, and immediately, the gas composition of the headspace was determined by gas chromatography-thermal conductivity detection (GC-TCD). Then, the bottles were incubated at 25 °C under continuous magnetic stirring (300 rpm) to prevent microalgae sedimentation. Light intensity of 900 μE $m^{-2}s^{-1}$ was continuously provided by visible LED lights (PHILLIPS, Spain).

In the test series I, four operational conditions were evaluated for each nanoparticle: 1) *C. sorokiniana* biomass and synthetic biogas A; 2) *C. sorokiniana* biomass with 10 mg L^{-1} of nanoparticles and biogas A; 3) *C. sorokiniana* and synthetic biogas B; 4) *C. sorokiniana* biomass with 10 mg L^{-1} of nanoparticles and biogas B. Each condition was run in triplicate. In test series II, the influence of different NPs concentrations (20 mg L^{-1}, 40 mg L^{-1}, and 70 mg L^{-1}) was assessed under biogas A headspace, 25 °C, magnetic stirring (300 rpm) and visible light 900 μE $m^{-2}s^{-1}$. A control containing only *C. sorokiniana* and biogas A was conducted. Each condition was run in triplicate. Finally, in test series III, the influence of different NPs concentrations (20 mg L^{-1}, 40 mg L^{-1}, and 70 mg L^{-1}) was assessed under biogas A headspace, 25 °C, magnetic stirring (300 rpm) and visible light (900 μE $m^{-2}s^{-1}$) + UV light (λ 315–350 nm, 10 W m^{-2}). A control containing only *C. sorokiniana* biomass and biogas A was conducted. Each condition was run in triplicate.

2.4. Analytical procedures

Microalgae Biomass productivity (Px) was calculated according to Eq. (1):

$$Px = \frac{DW_1 - DW_0}{t_1 - t_0} \quad (1)$$

where Px is biomass productivity (g L^{-1} d^{-1}), DW_1 and DW_0 are the biomass dry weight (g L^{-1}) at time t_1 and t_0 (d).

The biogas composition in the headspace of the bottles (CH_4, CO_2, H_2S and O_2) was determined two times per day by GC-TCD (Bruker) according to [9]. pH was determined at the beginning and at the end of the experiment (SensION^{TM} + PH3 pHmeter, HACH, Spain). The dissolved IC concentrations were determined at the beginning and at the end of the experiments using a Shimadzu TOC-VCSH analyzer (Japan) equipped with a TNM-1 chemiluminescence module. Microalgae growth was determined daily by optical density at 750 nm (OD_{750}) using a Shimadzu spectrophotometer (Japan). TSS concentrations were determined according to standard methods [24]. The biomass obtained from test series II and III was harvested (10000 rpm, 4 °C) and freeze-dried for further macromolecular characterization. The carbohydrate content was determined according to [25], while the lipid content was determined gravimetrically following biomass extraction with chloroform:methanol (2:1 v v^{-1}) as described elsewhere [26]. Physisorption analysis was conducted in an ASAP 2050 (Micromeritics, USA) at 77 K using nitrogen to determine the surface area, pore volume and avarage pore diameter of the NPs. Scanning electron microscopy (SEM) (JEOL JSM-6490LV) and energy-dispersive spectroscopy (EDS) (EDX-700/800, Hitachi, Japan) were carried out to determine the surface morphology and elemental composition of the target NPs.

2.5. Statistical analysis

The results are presented as mean values ± standard deviation. An analysis of variance (ANOVA) followed by Tuckey's test considering $\alpha = 0.05$ was performed to assess the influence of NPs on microalgae metabolism.

3. Results and discussion

3.1. Characterization of nanoparticles

SEM micrographs show the morphology of the NPs herein used (Fig. 1). The Fe_2O_3 NPs exhibited a particle size of 25 nm and nanorod morphology, which has been previously reported to exhibit a high specific surface area, and better electrochemical and magnetic properties compared to other Fe_2O_3 morphologies [27–29]. The CALPECH NPs presented particle size ranging from 50 to 70 nm and were agglomerated, which is in accordance to [30,31]. Finally, the SMALLOPS NPs exhibited the highest particle size (150 nm) and were also agglomerated. The EDS analysis showed the presence of elements such as P, K, Ca and S in CALPECH and SMALLOPS NPs (Fig. S2 and S3, respectively), which could play a key role to stimulate microalgae growth. Additionally, the EDS analysis revealed a Fe content of 7.26 % (wt. %) in CALPECH NPs, whereas a Fe content of 31.38 (wt. %) was recorded in SMALLOPS NPs. At this point, it is important to highlight that the difference in Fe content between the CALPECH and SMALLOPS NPs could influence differently *C. sorokiniana* growth and metabolism.

The BET surface area is a typical parameter for the selection of adsorbents, and the higher the surface area, the better the adsorbent capacity [32]. The BET surface areas of the NPs herein used were 32.07, 27.26 and 5.45 $m^{-2}g^{-1}$ for Fe_2O_3, CALPECH and SMALLOPS respectively, suggesting that Fe_2O_3 and CALPECH NPs could act as better gas adsorbents than SMALLOPS NPs. The lowest surface area of the SMALLOPS NPs can be attributed to the higher particle size, and the agglomeration of the NPs due to Van Der Waals forces [33]. Additionally, the pore volume of a material has been more strongly correlated to its adsorption capacity [32]. In this particular study, the pore volume of the NPs used was 0.38, 0.28 and 0.03 cm^3g^{-1} for Fe_2O_3, CALPECH and SMALLOPS NPs, respectively. Thus, the latter also suggested that Fe_2O_3 NPs can act as better adsorbents than CALPECH and SMALLOPS NPS. Finally, the pore diameter of Fe_2O_3, CALPECH and SMALLOPS NPs was 47.46, 41.47 and 27.45 nm, respectively. According to the IUPAC classification, the three NPs herein used represented mesoporous materials. Fe_2O_3 and mesoporous carbon materials are known for their CO_2 adsorption capacities [34,35]. The properties observed in the materials herein used suggest that Fe_2O_3 NPs closely followed by CALPECH NPs could positively impact CO_2 adsorption, thus resulting in an increased *C. sorokiniana* growth rate due to a higher CO_2 availability. However, the nature of the NPs could play an important role on microalgae metabolism.

3.2. Influence of biogas composition on C. sorokiniana growth and CO_2 removal

The cumulative CO_2 consumption and cumulative O_2 production in the headspace of the bottles and the cumulative OD_{750} served as indicators of *C. sorokiniana* growth (Fig. 2). *C. sorokiniana* growth was inhibited in all the assays containing biogas B in the headspace. Indeed, the presence of sulfur oxidizing bacteria is necessary to create a symbiosis with microalgae and prevent H_2S toxicity, since sulfur oxidizing bacteria utilize the O_2 produced by microalgae to oxidize the H_2S contained in biogas into SO_4^{2-} [4,36]. It has been stated elsewhere [37] that the high dissolved oxygen concentrations achieved in algal cultures can mediate the oxidation of H_2S. In the present study, the low *C. sorokiniana* concentrations could not release enough oxygen to oxidize the H_2S contained in biogas B, resulting in biomass inhibition.

On the other hand, biogas A did not inhibit the growth of *C. sorokiniana*. The addition of Fe_2O_3, CALPECH and SMALLOPS NPs did not support an enhancement in the cumulative CO_2 consumption likely due to the low NPs concentration tested. Interestingly, the addition of Fe_2O_3 and CALPECH NPs induced a slightly higher cumulative O_2 production of 7 % ($p = 0.007$) and 5 % ($p = 0.016$), respectively (Fig. 2d and 2e), confirming that these NPs positively influenced *C. sorokiniana* growth. The OD_{750} of the culture broths containing Fe_2O_3 increased by 33 % (Fig. 2g), whereas the assays containing CALPECH NPs experienced an increase in OD_{750} during the exponential phase (Fig. 2h). Lei and collaborators [38] investigated the effect of iron NPs on green algae and observed that Fe oxidation state played an important role on microalgae growth and growth inhibition decreased with the oxidation of NPs. Vaz and collaborators [19] demonstrated that the addition of polymeric nanofibers containing Fe_2O_3 NPs improved CO_2 biofixation of *Chlorella fusca.* In the present study, the enhancement in O_2 production and cumulative OD_{750} induced by the addition of Fe_2O_3 NPs can be attributed to the fact that the NPs stimulated the growth of *C. sorokiniana,* since iron is one essential micronutrient for microalgae growth and acts as a cofactor in the electron transport system [39]. CALPECH and SMALLOPS NPs contained ZVI, whose addition to microalgae cultures induce contradictory effect in different microalgae species (i.e. *Chlorella pyrenoidosa* and *Desmodesmus subspicatus*) [38,40]. In this study, the addition of CALPECH NPs mediated a significant increment in O_2 production of 5.80 % ($p = 0.016$), and both O_2 production and OD_{750} were significantly enhanced ($p = 0.029$), during the exponential growth phase. The addition of SMALLOPS NPs did not induce an enhancement in O_2 production or in OD_{750} (Fig. 2f and 2i). The results herein obtained suggest that the ZVI content in the NPs can play a key role in microalgae growth, and the higher Fe content in SMALLOPS NPs could have interfered *C. sorokiniana* growth.

Biomass productivity (Px) was significantly enhanced ($p = 0.012$)

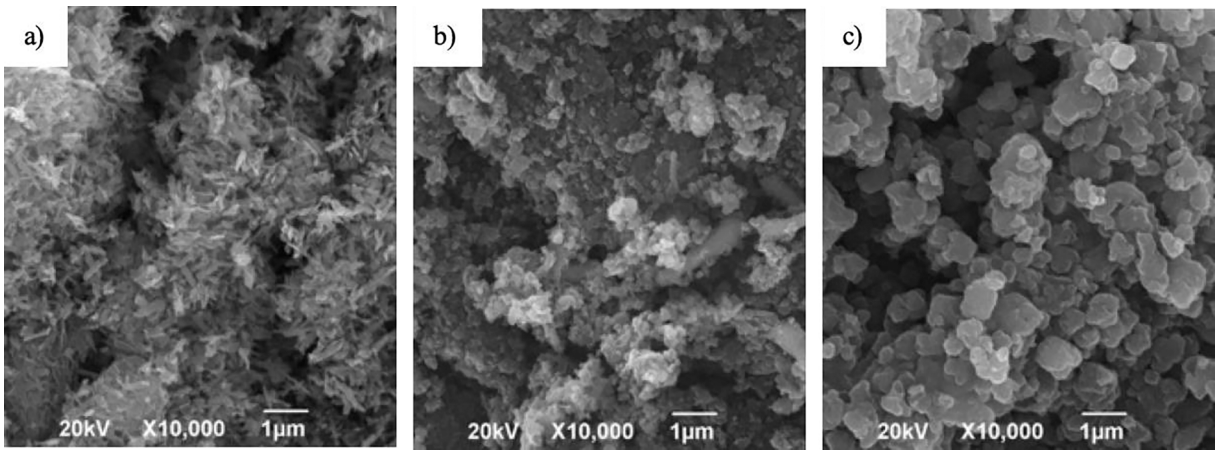

Fig. 1. SEM micrographs of a) Fe_2O_3, b) CALPECH and c) SMALLOPS nanoparticles.

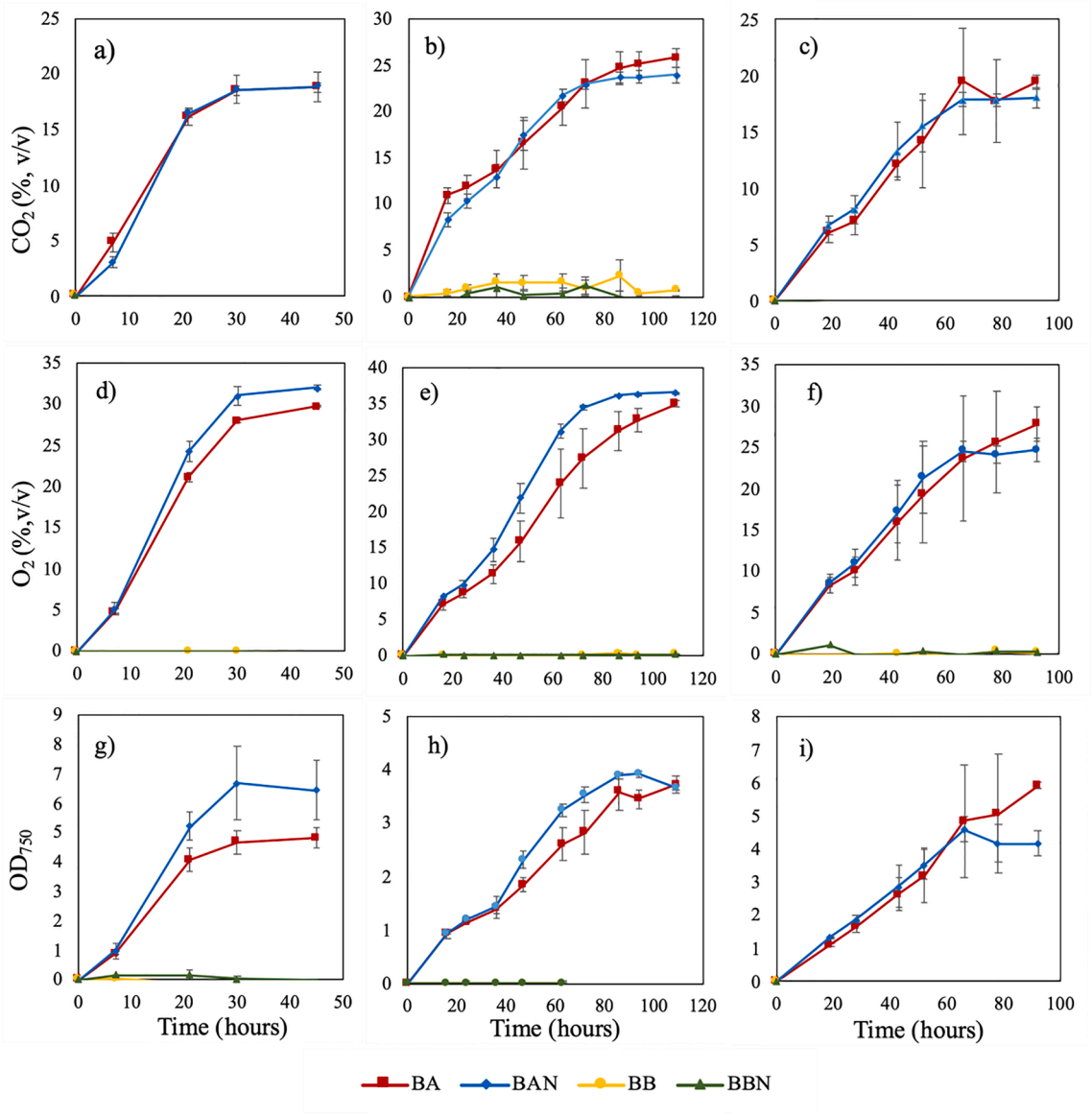

Fig. 2. Time course of the cumulative CO_2 consumption in the assays with 10 mg L^{-1} of a) Fe_2O_3 NPs, b) CALPECH NPs, c) SMALLOPS NPs; of the cumulative O_2 production in the assays with 10 mg L^{-1} of d) Fe_2O_3 NPs, e) CALPECH NPs, f) SMALLOPS NPs; and of culture absorbance (OD_{750}) in the assays with 10 mg L^{-1} of g) Fe_2O_3 NPs, h) CALPECH NPs, i) SMALLOPS NPs. NPs refers to the addition of nanoparticles; BA (squares) refers to the assays with biogas A; BAN (diamonds) refers to assays with biogas A and NPs; BB refers (circles) to the assays with biogas B; and BBN (triangles) refers to the assays with biogas B and NPs.

when CALPECH NPs were added (Table 1). Significant increases in the pH of the culture broths were recorded in the assays containing CALPECH ($p = 0.002$) and Fe_2O_3 ($p = 0.037$) NPs (Table 1). These results were in agreement with those of Pádrová and coworkers [40], who observed that low concentrations of ZVI NPs, ranging between 1.70 and 5.10 mg L^{-1}, stimulated the growth of *Desmodesmus subspicatus*, *Dunaliella salina*, *Parachlorella kessleri*, *Raphidocelis subcapitata*, *Nannochloropsis limnetica*, *Trachydiscus minutus* and *Arthrospira maxima*. The results herein obtained suggest that iron NPs influenced microalgal assimilation of CO_2.

Table 1
Biomass productivity and initial and final IC concentration in the *Chlorella sorokiniana* assays supplemented with 10 mg L^{-1} of the different NPs.

	Fe_2O_3		CALPECH		SMALLOPS	
	Control	10 mg L^{-1}	Control	10 mg L^{-1}	Control	10 mg L^{-1}
Px (g $L^{-1}d^{-1}$)	0.56 ± 0.07	0.79 ± 0.16	0.35 ± 0.08	0.59 ± 0.05	0.97 ± 0.12	0.76 ± 0.04
$IC_{initial}$ (mg L^{-1})	1417 ± 29	1426 ± 46	1468 ± 6	1486 ± 23	1497 ± 9	1453 ± 16
IC_{final} (mg L^{-1})	1108 ± 18	1036 ± 81	1203 ± 14	1144 ± 46	793 ± 12	819 ± 22
$pH_{initial}$	7.86 ± 0.07	7.81 ± 0.05	8.01 ± 0.84	7.84 ± 0.06	7.78 ± 0.02	7.75 ± 0.01
pH_{final}	9.00 ± 0.08	9.26 ± 0.13	8.93 ± 0.02	9.06 ± 0.03	8.79 ± 0.10	8.56 ± 0.12

3.3. Influence of nanoparticle concentration on C. sorokiniana growth and CO_2 removal under visible light

The addition of 40 and 70 mg L^{-1} of Fe_2O_3 NPs resulted in a significantly increased cumulative CO_2 consumption by 10 % and 26 %, respectively ($p = 0.00001$) (Fig. 3a). The cumulative O_2 production (Fig. 3d) and the OD_{750} (Fig. 3g) in the assay with 70 mg Fe_2O_3 L^{-1} were 19 % and 35 % higher than the control. No significant difference was

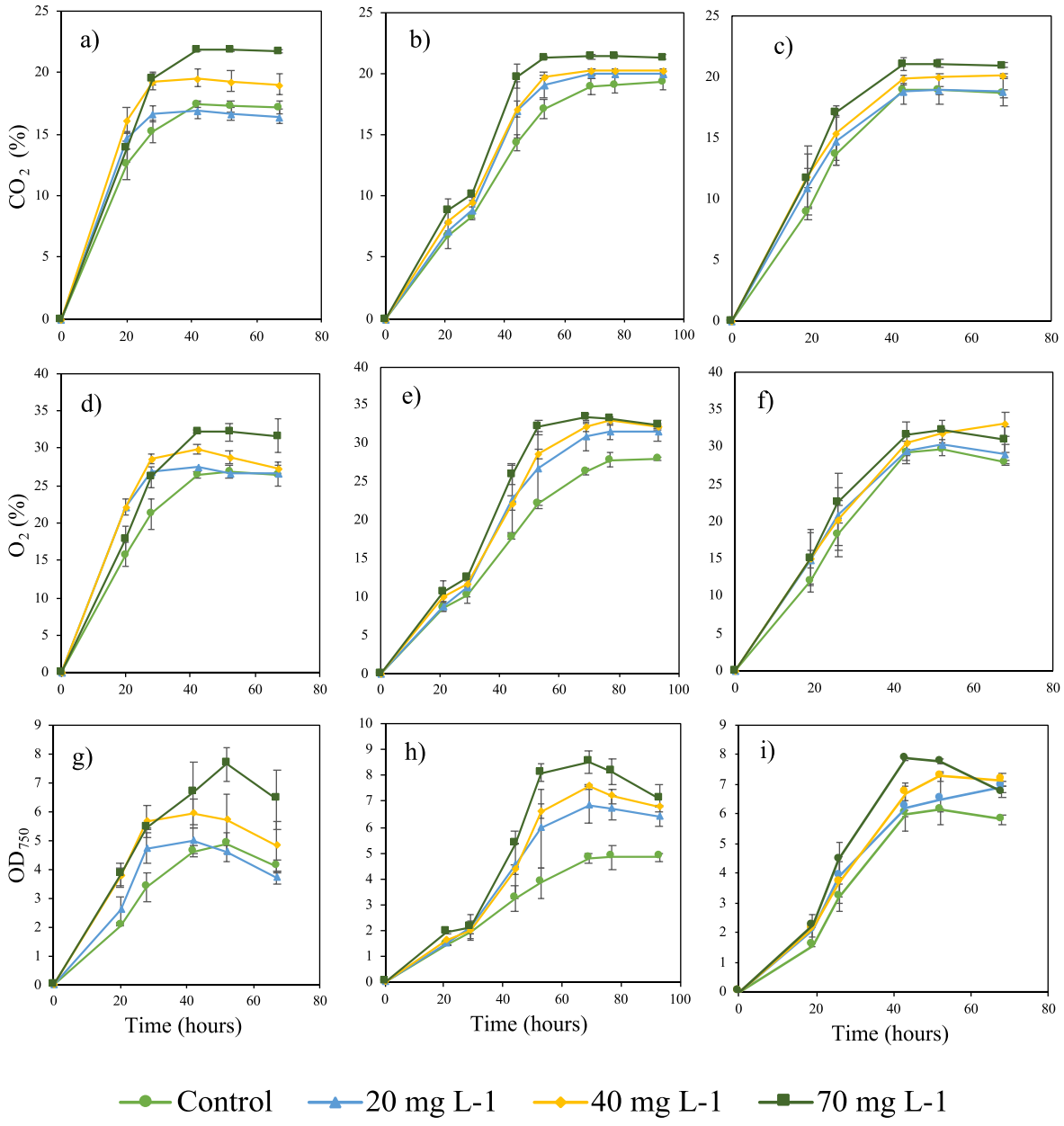

Fig. 3. Time course of the cumulative CO_2 consumptions in assays supplied with a) Fe_2O_3, b) CALPECH, c) SMALLOPS; of the cumulative O_2 production in the assays supplied with d) Fe_2O_3, e) CALPECH, e) SMALLOPS; and of the cumulative OD_{750} in the assays supplied with d) Fe_2O_3, e) CALPECH, e) SMALLOPS. The assays were carried out under visible light.

observed in Px ($p = 0.143$) (Table 2) or in IC ($p = 0.847$) concentration and pH ($p = 0.079$) (Table S1, S2) among the assays. These results disagreed with the observations of Rana and coworkers [41], who reported that the addition of Fe_2O_3 NPs resulted in growth inhibition of *C. sorokiniana* even at low concentrations (2 mg L^{-1}). The results herein obtained suggest that the toxicity of NPs in microalgae are not only species specific, but also the morphology and characteristics of the NPs can play a key role on microalgae growth [38]. The special morphology of the Fe_2O_3 NPs herein used neither inhibited microalgae growth nor delayed the exponential phase. On the contrary, the cumulative O_2 production increased at increasing NPs concentrations. This study confirmed that Fe_2O_3 NPs acted as CO_2 adsorbents and the higher CO_2 consumption in the 70 mg L^{-1} assays can be explained by the fact that CO_2 was adsorbed to the NP surface and more readily available for *C. sorokiniana* consumption. The addition of 70 mg L^{-1} of Fe_2O_3 increased the carbohydrate content of *C. sorokiniana* by 47 % compared to the control (10 %, dw) (Fig. 4a). The lipid content of *C. sorokiniana* decreased regardless of the concentration of NPs added. The latter suggest that the stress conditions caused by the addition of Fe_2O_3 induced lipid oxidation by reactive oxygen species (ROS) and the accumulation of carbohydrates as a protective response. These results were in agreement with Marchello and coworkers [42] who observed that the exposure of *C. sorokiniana* to TiO_2 NPs caused stress in microalgae cells, which resulted in a 140 % carbohydrate enhancement. Romero and coworkers [43] also observed a carbohydrate enhancement of up to 80 % in *Chlorella vulgaris* when exposed to Ag NPs.

The addition of 40 and 70 mg L^{-1} of CALPECH NPs resulted in a significantly enhanced CO_2 consumption ($p = 0.0006$) of 5 and 11 %, respectively (Fig. 4b). The O_2 production was significantly enhanced by 13, 15 and 16 % when dosing 20, 40 and 70 mg L^{-1}, respectively ($p =$

Table 2
Influence of the type and concentration of nanoparticles on biomass productivity as a function of the type of light source: visible light (white background) and visible light + UV light (grey background).

	P_X (g $L^{-1}d^{-1}$)		
	Fe_2O_3	*CALPECH*	*SMALLOPS*
Control	1.24 ± 0.12	0.81 ± 0.02	2.15 ± 0.16
20 mg L^{-1}	1.12 ± 0.09	1.75 ± 0.21	2.10 ± 0.41
40 mg L^{-1}	1.27 ± 0.35	1.10 ± 0.14	2.00 ± 0.27
70 mg L^{-1}	1.75 ± 0.49	1.67 ± 0.22	1.72 ± 0.13
Control	1.37 ± 0.19	2.01 ± 0.09	1.81 ± 0.19
20 mg L^{-1}	1.36 ± 0.33	1.92 ± 0.08	1.84 ± 0.05
40 mg L^{-1}	1.27 ± 0.16	2.15 ± 0.31	1.67 ± 0.11
70 mg L^{-1}	1.60 ± 0.43	2.07 ± 0.10	1.70 ± 0.25

0.00008) (Fig. 4e). The OD_{750} underwent enhancements of 33, 41 and 47 % when 20, 40 and 70 mg L^{-1} were added, respectively ($p = 0.0001$) (Fig. 4h). The Px was significantly higher ($p = 0.002$) when 70 mg L^{-1} were added (Table 2). The final IC concentrations and pH (Table S1, S2) confirmed the accelerated growth of *C. sorokiniana* mediated by the addition of CALPECH NPs. The addition of CALPECH NPs resulted in a positive effect on *C. sorokiniana* regardless of the concentration added. However, 70 mg L^{-1} supported the highest enhancements among all the concentrations tested. The carbohydrate content and the lipid content of *C. sorokiniana* was 12 % and 11 % (% dw) respectively, without the addition of NPs. The addition of 70 mg L^{-1} of CALPECH NPs significantly increased ($p = 0.0006$) the carbohydrate and lipid content by 56 % and 25 % respectively, whereas no significant changes were observed in the presence of the other concentrations tested (Fig. 4b). This suggested that CALPECH NPs were not toxic to *C. sorokiniana* likely due to the low iron content of the NPs. The main iron source of these particular NPs is ZVI which has previously shown to be less toxic for microalgae species compared to other iron NPs, also provides a source of iron that increases cell growth and induces metabolic changes in some microalgae species [40,44]. Pádrová and coworkers [40] observed that 5.1 mg L^{-1} of ZVI stimulated the growth of *Arthrospira maxima*. In another study, Kadar and coworkers [44] showed that *Pavlova lutheri*, *Isochrysis galbana* and *Tetraselmis suecica* preferred ZVI NPs over EDTA-Fe. Thus, it can be hypothesized that CALPECH NPs accelerated the metabolism of *C. sorokiniana*. The high CO_2 availability, induced by the high CO_2 concentrations in the headspace of the bottles, led to an activation of the RuBisCO enzyme, which is the rate-limiting enzyme in the Calvin cycle [45]. The activation of the latter enzyme can result in an increased photosynthetic efficiency and CO_2 fixation [46]. This enhanced CO_2 availability was mainly attributed to the porosity of the NPs, since part of the CO_2 remained adhered to the surface of the NPs and was released by the so-called "shuttle" effect [14].

The addition of 70 mg L^{-1} of SMALLOPS NPs entailed an increased cumulative CO_2 (12 % higher than the control) consumption ($p = 0.005$). The O_2 production in tests supplied with 40 mg L^{-1} was 15 % higher than the control, while the assays containing 70 mg L^{-1} of SMALLOPS NPs did not experience an O_2 production enhancement. It is well known that iron NPs exhibit the potential to induce the formation of ROS by Fenton reactions, Fenton-like reactions, Haber-Weiss reactions or even more complex reactions [39,41]. In these reactions O_2 reacts with the released Fe^+ ions to form ROS, hence, the O_2 photosynthetically produced could have led to the formation of ROS. The OD_{750} was 19, 22 an 15 % higher than the control when 20, 40 and 70 mg L^{-1} were added ($p = 0.003$) respectively, confirming the increased *C. sorokiniana* growth by the addition of SMALLOPS NPs. However, Px did not experience significant differences ($p = 0.276$) among the assays. The final IC concentrations and pH values (Table S1 and S2) confirmed that the addition of 40 mg L^{-1} of SMALLOPS NPs stimulated *C. sorokiniana* growth, suggesting that this concentration could be the optimal for *C. sorokiniana*. The carbohydrates content of *C. sorokiniana* without NPs was 7 % (dw) and increased by 66, 42 and 91 % when 20, 40 and 70 mg L^{-1} were added, respectively. The lipid content of the microalgal biomass without NPs was 14 % (dw) and increased as well with the addition of NPs. The assays containing 40 mg L^{-1} experienced an increase of 32 % (Fig. 4c), which was the higher lipid content herein recorded. The latter suggest that the addition of SMALLOPS NPs resulted in accelerated microalgae metabolism and in the production of high value biomass. The addition of SMALLOPS NPs seems to have induced a formation of ROS directly proportional to the percentage of iron content in the NPs, which influenced lipid accumulation in *C. sorokiniana*. The lipid content in the assays provided with 70 mg L^{-1} decreased, likely because the concentration of ROS was higher than the tolerated by *C. sorokiniana,* resulting in the oxidation of lipids as a mechanism of defense. The higher iron content in SMALLOPS NPs induced lipid accumulation in

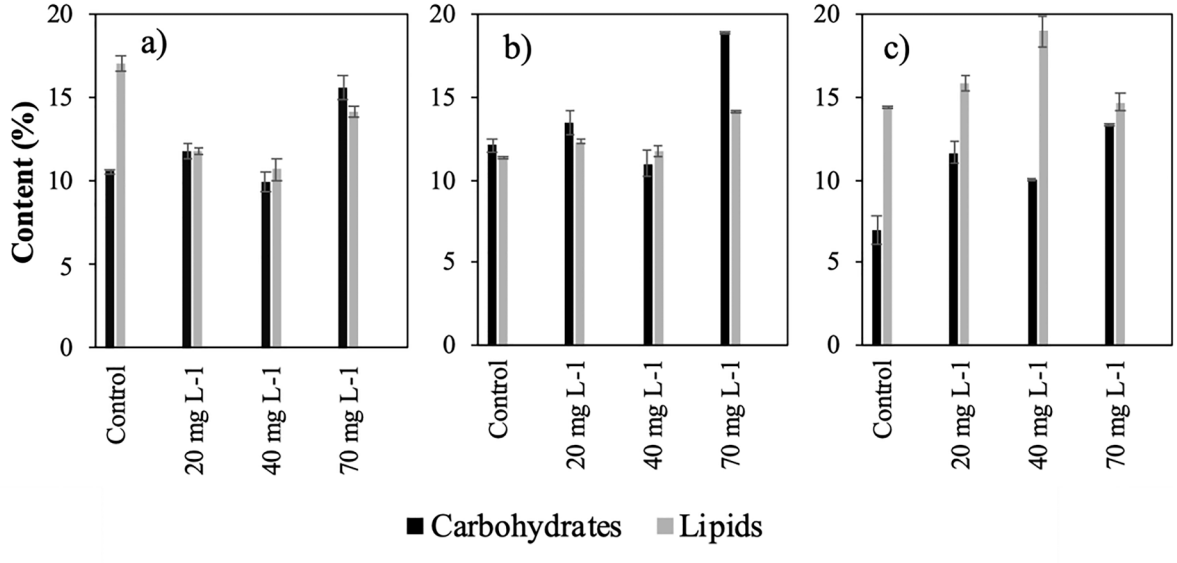

Fig. 4. Influence of the concentration of a) Fe_2O_3 NPs; b) CALPECH NPs; c) SMALLOPS NPs on the carbohydrate (black) and lipid (grey) content of microalgae biomass at the end of the assays under visible light.

C. sorokiniana, which represents an innovative strategy to produce lipid-enriched biomass at relatively low NPs concentrations.

3.4. Influence of nanoparticle concentration on *C. sorokiniana* growth and CO_2 removal under visible + UV light

Yang and coworkers [20] recently studied the effect of graphene oxide quantum dots on *Chlorella pyrenoidosa* under UV light and observed a positive effect of the growth and lipid production of this microalgae. Similarly, Dinc and coworkers [47] demonstrated that the addition of Se NPs to microalgae reduced UV-stress effects in *C. vulgaris*. The present study assessed the influence of UV light supplementation to visible light at different concentrations of the Fe_2O_3, CALPECH and SMALLOPS NPs.

The addition of Fe_2O_3 NPs under visible light supplemented with UV light exerted the same effects than visible light. Indeed, the concentrations of 40 and 70 mg L^{-1} resulted in an increase in the cumulative CO_2 consumption of 13 and 23 %, respectively (p = 0.00004) (Fig. 5a). However, while the assays containing 40 mg L^{-1} led to an enhanced O_2 production (p = 0.019) (Fig. 5d), the assays with 70 mg L^{-1} did not show a significant difference compared to the control tests (p = 0.162). The OD_{750} (p = 0.148) (Fig. 4g), Px (p = 0.602) (Table 2) and the final IC concentration (p = 0.585) (Table S1) did not show any significant differences among the assays. The obtained results suggested that the exposure to UV light in the presence of Fe_2O_3 NPs did not exert a toxic effect on *C. sorokiniana* since the growth was not inhibited and no retarded exponential growth was observed, contrary to the results obtained by Bibi and coworkers [48]. The carbohydrate content was significantly increased (p = 0.00003) by 300, 190 and 530 % under 20, 40 and 70 mg Fe_2O_3 L^{-1}, respectively (Fig. 6a), while the lipid content decreased regardless of the concentration of Fe_2O_3 NPs. The addition of Fe_2O_3 NPs under UV + visible light mediated the same mechanisms than visible light. Fe_2O_3 NPs under UV light exposure (<260 nm) increased their oxidation effectiveness (Photo-Fenton process) [49] however, in

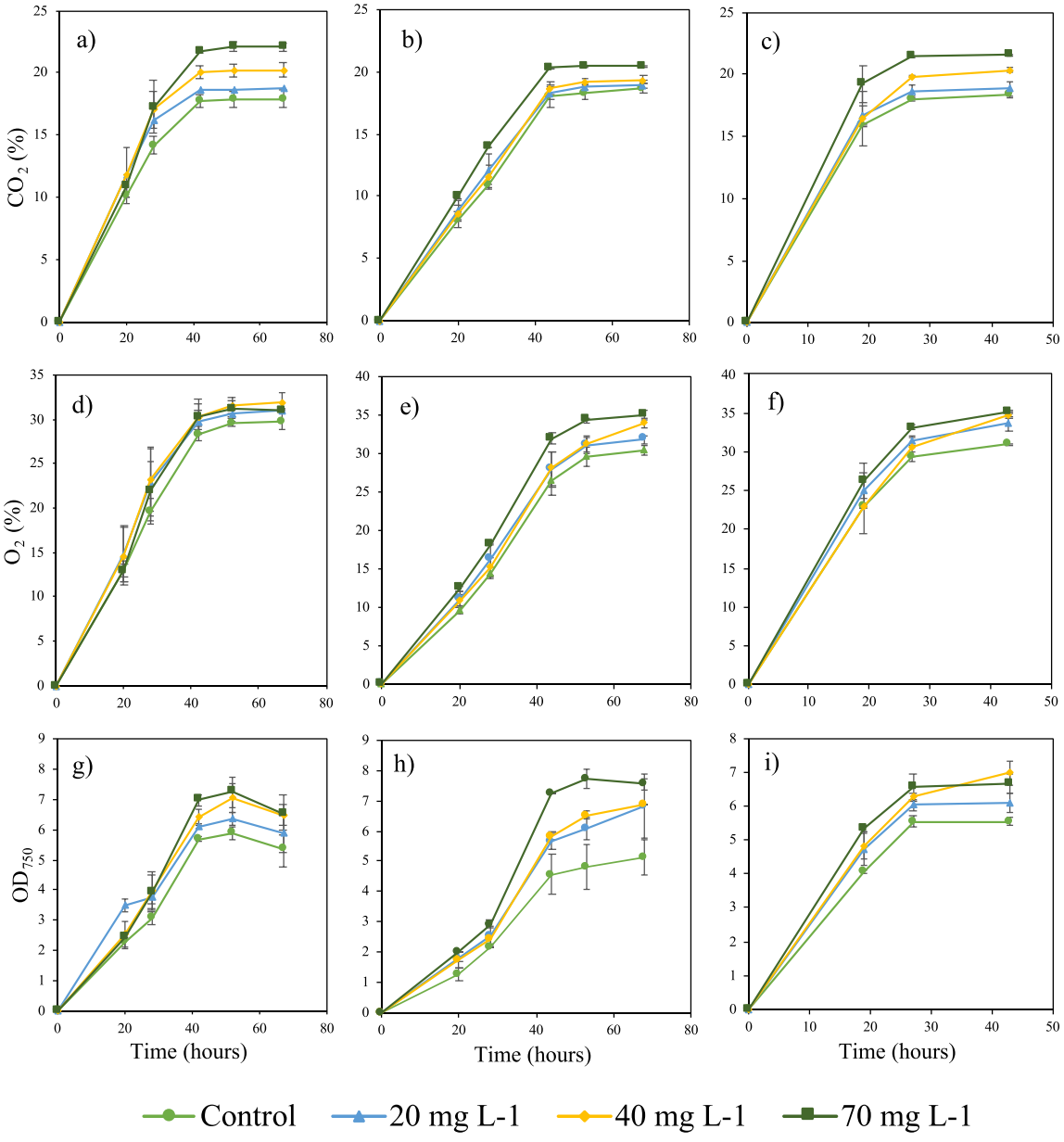

Fig. 5. Time course of the cumulative CO_2 consumptions in assays with a) Fe_2O_3, b) CALPECH, c) SMALLOPS; cumulative O_2 production in assays with d) Fe_2O_3, e) CALPECH, e) SMALLOPS; and cumulative OD_{750} in assays with d) Fe_2O_3, e) CALPECH, e) SMALLOPS. The assays were carried out under visible light + UV light.

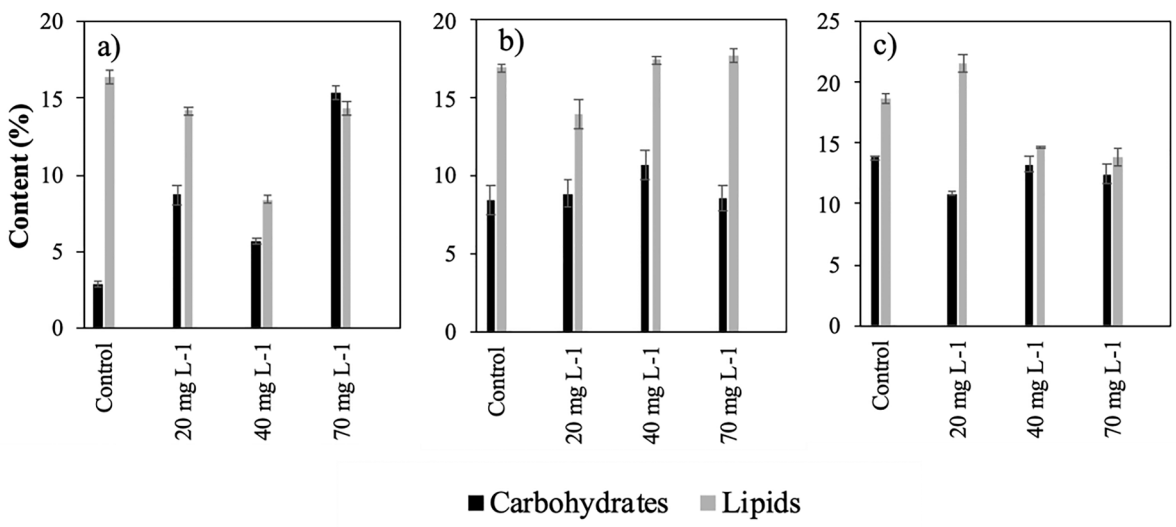

Fig. 6. Influence of the concentration of a) Fe_2O_3 NPs; b) CALPECH NPs; c) SMALLOPS NPs on the carbohydrate (black) and lipid (grey) content of microalgae biomass at the end of the assays under visible light + UV light.

the present study, the UV light exposure coupled to the addition of Fe_2O_3 NPs resulted in lower lipid contents in *C. sorokiniana* compared to the lipid contents under visible light. The lower lipid content in *C. sorokiniana* (<16 %, dw) was herein attributed to a response to UV radiation. The significant increase in carbohydrate content compared to the control (2 %, dw) ($p = 0.00003$) suggested the occurrence of stress conditions caused by the NPs, regardless of the type of light, and can be attributed to an increased respiration and higher carbohydrates requirements for energy production [43].

The addition of 40 and 70 mg L^{-1} of CALPECH NPs resulted in a 4 and 9 % higher cumulative CO_2 consumption compared to the control assays ($p = 0.0004$), respectively (Fig. 5b). The O_2 production increased with NPs concentration, with enhancements of 7, 11 and 17 % at 20, 40 and 70 mg L^{-1} respectively ($p = 0.0009$), compared to the control assays (Fig. 5e). The increased photosynthetic activity of *C. sorokiniana* was also supported by the final OD_{750}, which were 33, 34 and 47 % higher at 20, 40 and 70 mg L^{-1} ($p = 0.009$) respectively, compared to the control tests (Fig. 5h). Even though Px (Table 2) did not exhibit a significant difference among the assays ($p = 0.448$), the exponential growth phase was slightly increased by the addition of 70 mg L^{-1} of CALPECH NPs. The final IC ($p = 0.029$) and pH ($p = 0.0000009$) (Table S1 and S2) supported the accelerated growth of *C. sorokiniana.* The carbohydrate and lipid contents of the control were 8.5 % and 17 % (% dw) respectively, and did not exhibit significant differences by the addition of NPs ($p = 0.179$) (Fig. 6b). From the results herein obtained, it can be said that the UV light exposure reduced the beneficial effects of CALPECH NPs in terms of accumulation of macromolecules. However, since the cumulative CO_2, O_2 and OD_{750} were similar to the assays carried out under visible light, the results under UV light exposure support the theory that the enhanced CO_2 availability by the addition of CALPECH NPs was likely due to the adhesion of the gas to the surface of the NPs. The enhancement in the lipid content can be attributed to the formation of ROS mediated by the iron source of the NPs. Even though the mechanism of interaction of the NPs under UV light is not very clear, UV light exposure could have reduced the activity of the iron source explaining the reduced lipid and carbohydrate accumulation under UV exposure. Moreover, Dinc and coworkers [47] observed that Se NPs are effective at scavenging free radicals under UV exposure, thus the iron source of the CALPECH NPs could have the same response under UV radiation as well.

The addition of SMALLOPS NPs resulted in an increased cumulative CO_2 consumption of 10 % and 17 % when 40 and 70 mg L^{-1} were added, respectively ($p = 0.003$) (Fig. 5c). The O_2 production was increased regardless of the concentration of NPs, with enhancements of 8, 11 and 12 % for 20, 40 and 70 mg L^{-1}, respectively ($p = 0.002$) (Fig. 5f). The cumulative OD_{750} confirmed the enhanced growth of *C. sorokiniana*, where the addition of 40 and 70 mg L^{-1} resulted in 25 and 20 % higher cumulative OD_{750} than the control ($p = 0.002$) (Fig. 5i). Even if no significant differences in Px were recorded ($p = 0.577$) (Table 2), the final IC ($p = 0.0008$) concentration and pH ($p = 0.0002$) values (Table S1 and S2) confirmed the accelerated microalgae growth in the assays containing 40 and 70 mg L^{-1} of SMALLOPS NPs. SMALLOPS NPs supported similar *C. sorokiniana* growth patterns under visible light and UV–visible light, which suggested that the stimulated *C. sorokiniana* growth can be attributed to the interaction between the carbon coat of the NPs and the gaseous CO_2. The iron content of the NPs is the responsible of the lipid/carbohydrate content, since the iron ions can led to the formation of ROS through the Fenton process [39]. SMALLOPS NPs lipid content without the NPs was 19 % (dw). The addition of 40 and 70 mg L^{-1} of NPs induced lipid oxidation (Fig. 6a and 6b, respectively), whereas the lipid content of *C. sorokiniana* was enhanced by 11 % with the addition of 20 mg L^{-1} ($p = 0.0004$) (Fig. 6c). The latter suggest that the iron source of SMALLOPS NPs enhanced their oxidative activity by the exposure of UV light [49], and 20 mg L^{-1} of NPs induced an increase in *C. sorokiniana* lipid content as a mechanism of protection. Lipid oxidation could have occurred at 40 and 70 mg L^{-1} due to the higher ROS concentration present in the culture media. It has been previously reported that ZVI NPs act as electron donors to catalyze a wide range of different reactions, and this particular NPs exhibit a better bioavailability compared to other iron NPs [40]. Positive effects of ZVI NPs have been reported at concentrations below 5.1 mg L^{-1} [40,44], thus, the latter explains the fact that the higher content of Fe in SMALLOPS NPs lead to the formation of ROS whereas the low concentration of Fe in CALPECH NPs resulted in biomass enhancements. Under UV radiation, the iron source of CALPECH NPs could act as UV scavengers, whereas the high concentration of Fe in SMALLOPS NPs under UV light likely mediated the formation of ROS.

Finally, the results obtained from UV-light exposure confirmed the fact that the increased CO_2 availability was due to the porosity of the NPs, and the CO_2 concentration was directly correlated to the NPs concentration. The increased CO_2 accumulation in the headspace did not increase IC concentration in the bottles containing NPs, suggesting that both shuttle and hydrodynamic effect could have occurred. Indeed, the CO_2 could have been adhered to the NPs surface and then released to the headspace of the bottles. Then, the presence of the NPs created an

hydrodynamic effect as described in [14], which facilitated the transfer of CO_2 to microalgae. On the other hand, the iron source was the responsible for the macromolecule accumulation/decrease in *C. sorokiniana*.

4. Conclusions

The mesoporous nature of the three different nanoparticles improved CO_2 availability and adsorption to *Chlorella sorokiniana* cultures regardless of their chemical composition. The addition of iron nanoparticles resulted in an enhanced *C. sorokiniana* growth regardless of the concentration and the type of nanoparticles tested. The results obtained suggest that both shuttle and hydrodynamic effects could have occurred during the cultivation of *C. sorokiniana*. The different iron sources of each nanoparticle influenced differently *C. sorokiniana* metabolism and was the responsible for carbohydrates/lipids accumulation. UV light exposure confirmed the fact that the higher CO_2 availability was likely due to the physical properties of the nanoparticles. However, UV light exposure induced lipid oxidation when Fe_2O_3 and SMALLOPS nanoparticles were added as a result of their higher iron content. Mesoporous nanoparticles can be considered as an effective technology to improve CO_2 consumption during photosynthetic biogas upgrading.

CRediT authorship contribution statement

Laura Vargas-Estrada: Methodology, Writing – original draft. **Edwin G. Hoyos:** Methodology. **P.J. Sebastian:** Writing – review & editing. **Raúl Muñoz:** Supervision, Writing – review & editing.

Declaration of Competing Interest

The authors declare that they have no known competing financial interests or personal relationships that could have appeared to influence the work reported in this paper.

Data availability

The data that has been used is confidential.

Acknowledgements

This work was supported by the Regional Government of Castilla y León and the EU-FEDER (CLU 2017-09, CL-EI-2021-07, UIC 315). Sebastian P.J. acknowledges the financial support from DGAPA-UNAM through the project IN108922. Laura Vargas-Estrada would like to acknowledge CONACYT for her PhD grant. The authors gratefully acknowledge CALPECH and SMALLOPS for providing the nanoparticles.

Appendix A. Supplementary data

Supplementary data to this article can be found online at https://doi.org/10.1016/j.fuel.2022.126362.

References

[1] Ángeles R, Vega-Quiel MJ, Batista A, Fernández-Ramos O, Lebrero R, Muñoz R. Influence of biogas supply regime on photosynthetic biogas upgrading performance in an enclosed algal-bacterial photobioreactor. Algal Res 2021:57. https://doi.org/10.1016/j.algal.2021.102350.
[2] Rodero MDR, Carvajal A, Arbib Z, Lara E, de Prada C, Lebrero R, et al. Performance evaluation of a control strategy for photosynthetic biogas upgrading in a semi-industrial scale photobioreactor. Bioresour Technol 2020;307:123207.
[3] Rodero MDR, Lebrero R, Serrano E, Lara E, Arbib Z, García-Encina PA, et al. Technology validation of photosynthetic biogas upgrading in a semi-industrial scale algal-bacterial photobioreactor. Bioresour Technol 2019;279:43–9.
[4] Franco-Morgado M, Toledo-Cervantes A, González-Sánchez A, Lebrero R, Muñoz R. Integral (VOCs, CO2, mercaptans and H2S) photosynthetic biogas upgrading using innovative biogas and digestate supply strategies. Chem Eng J 2018;354:363–9. https://doi.org/10.1016/j.cej.2018.08.026.
[5] Toledo-Cervantes A, Serejo ML, Blanco S, Pérez R, Lebrero R, Muñoz R. Photosynthetic biogas upgrading to bio-methane: boosting nutrient recovery via biomass productivity control. Algal Res 2016;17:46–52. https://doi.org/10.1016/J.ALGAL.2016.04.017.
[6] Xu J, Zhao Y, Zhao G, Zhang H. Nutrient removal and biogas upgrading by integrating freshwater algae cultivation with piggery anaerobic digestate liquid treatment. Appl Microbiol Biotechnol 2015;99:6493–501. https://doi.org/10.1007/s00253-015-6537-x.
[7] Meier L, Pérez R, Azócar L, Rivas M, Jeison D. Photosynthetic CO2 uptake by microalgae: an attractive tool for biogas upgrading. Biomass Bioenergy 2015;73:102–9. https://doi.org/10.1016/J.BIOMBIOE.2014.10.032.
[8] Marín D, Carmona-Martínez AA, Lebrero R, Muñoz R. Influence of the diffuser type and liquid-to-biogas ratio on biogas upgrading performance in an outdoor pilot scale high rate algal pond. Fuel 2020;275:117999. https://doi.org/10.1016/j.fuel.2020.117999.
[9] Posadas E, Serejo ML, Blanco S, Pérez R, García-Encina PA, Muñoz R. Minimization of biomethane oxygen concentration during biogas upgrading in algal–bacterial photobioreactors. Algal Res 2015;12:221–9. https://doi.org/10.1016/J.ALGAL.2015.09.002.
[10] Rodero MDR, Severi CA, Rocher-Rivas R, Quijano G, Muñoz R. Long-term influence of high alkalinity on the performance of photosynthetic biogas upgrading. Fuel 2020;281:118804.
[11] Bose A, Lin R, Rajendran K, O'Shea R, Xia Ao, Murphy JD. How to optimise photosynthetic biogas upgrading: a perspective on system design and microalgae selection. Biotechnol Adv 2019;37(8):107444.
[12] Kumar R, Mangalapuri R, Ahmadi MH, Vo DVN, Solanki R, Kumar P. The role of nanotechnology on post-combustion CO2 absorption in process industries. Int J Low-Carbon Technol 2020;15:361–7. https://doi.org/10.1093/IJLCT/CTAA002.
[13] Choi ID, Lee JW, Kang YT. CO2 Capture/Separation Control by SiO2 Nanoparticles and Surfactants. Sep Sci Technol 2015;50:772–80. https://doi.org/10.1080/01496395.2014.965257.
[14] Kluytmans JHJ, van Wachem BGM, Kuster BFM, Schouten JC. Mass transfer in sparged and stirred reactors: influence of carbon particles and electrolyte. Chem Eng Sci 2003;58:4719–28. https://doi.org/10.1016/j.ces.2003.05.004.
[15] Alper E, Öztürk S. The effect of activated carbon loading on oxygen absorption into aqueous sodium sulphide solutions in a slurry reactor. Chem Eng J 1986;32:127–30. https://doi.org/10.1016/0300-9467(86)80061-2.
[16] Liang SXT, Wong LS, Dhanapal ACTA, Djearamane S. Toxicity of metals and metallic nanoparticles on nutritional properties of microalgae. Water Air Soil Pollut 2020:231. https://doi.org/10.1007/s11270-020-4413-5.
[17] He M, Yan Y, Pei F, Wu M, Gebreluel T, Zou S, et al. Improvement on lipid production by *Scenedesmus obliquus* triggered by low dose exposure to nanoparticles. Sci Rep 2017;7:1–12. https://doi.org/10.1038/s41598-017-15667-0.
[18] Jeon HS, Park SE, Ahn B, Kim YK. Enhancement of biodiesel production in *Chlorella vulgaris* cultivation using silica nanoparticles. Biotechnol Bioprocess Eng 2017;22:136–41. https://doi.org/10.1007/s12257-016-0657-8.
[19] da Silva Vaz B, Alberto Vieira Costa J, Greque de Morais M. Physical and biological fixation of CO2 with polymeric nanofibers in outdoor cultivations of *Chlorella fusca* LEB 111. Int J Biol Macromol 2020;151:1332–9.
[20] Yang L, Su Q, Si B, Zhang Y, Zhang Y, Yang H, et al. Enhancing bioenergy production with carbon capture of microalgae by ultraviolet spectrum conversion via graphene oxide quantum dots. Chem Eng J 2022;429:132230.
[21] Norouzi A, Nezamzadeh-Ejhieh A. α-Fe2O3/Cu2O heterostructure: Brief characterization and kinetic aspect of degradation of methylene blue. Phys B Condens Matter 2020:599. https://doi.org/10.1016/j.physb.2020.412422.
[22] Borde X, Guieysse B, Delgado O, Muñoz R, Hatti-Kaul R, Nugier-Chauvin C, et al. Synergistic relationships in algal-bacterial microcosms for the treatment of aromatic pollutants. Bioresour Technol 2003;86(3):293–300.
[23] Guieysse B, Borde X, Muñoz R, Hatti-Kaul R, Nugier-Chauvin C, Patin H, et al. Influence of the initial composition of algal-bacterial microcosms on the degradation of salicylate in a fed-batch culture. Biotechnol Lett 2002;24:531–8. https://doi.org/10.1023/A:1014847616212.
[24] APHA-AWWA-WPCF. Standard Methods for the Examination of Water and Wastewater. 20th ed. Washington: 1999. doi: 10.2105/ajph.56.4.684-a.
[25] Dubois M, Smith F, Rebers PA, Gilles KA, Hamilton JK. Colorimetric method for determination of sugars and related substances. Anal Chem 1956;28:350–6. https://doi.org/10.1021/ac60111a017.
[26] Ángeles R, Arnaiz E, Gutiérrez J, Sepúlveda-Muñoz CA, Fernández-Ramos O, Muñoz R, et al. Optimization of photosynthetic biogas upgrading in closed photobioreactors combined with algal biomass production. J Water Process Eng 2020;38:101554.
[27] Bazrafshan H, Alipour Tesieh Z, Dabirnia S, Shajareh Touba R, Manghabati H, Nasernejad B. Synthesis of novel α-Fe2O3 nanorods without surfactant and its electrochemical performance. Powder Technol 2017;308:266–72. https://doi.org/10.1016/j.powtec.2016.12.015.
[28] Rao BN, Padmaraj O, Kumar PR, Venkateswarlu M, Madhusudhan Rao V, Satyanarayana N. Synthesis of hematite α-Fe 2 O 3 nanospheres for lithium ion battery applications. AIP Conf Proc 2015;1665:17806–12. https://doi.org/10.1063/1.4917849.
[29] Powell CD, Lounsbury AW, Fishman ZS, Coonrod CL, Gallagher MJ, Villagran D, et al. Nano-structural effects on Hematite (α-Fe2O3) nanoparticle radiofrequency heating. Nano Converg 2021;8(1). https://doi.org/10.1186/s40580-021-00258-7.
[30] Correcher R, Budyk Y, Fullana A. Role of gallic acid in the synthesis of carbon-encapsulated iron nanoparticles by hydrothermal carbonization: selecting iron oxide composition. ACS Omega 2021;6(44):29547–54.

[31] Munoz M, Nieto-Sandoval J, Álvarez-Torrellas S, Sanz-Santos E, Calderón B, de Pedro ZM, et al. Carbon-encapsulated iron nanoparticles as reusable adsorbents for micropollutants removal from water. Sep Purif Technol 2021;257:117974.
[32] Zhang R, Zeng L, Wang F, Li X, Li Z. Influence of pore volume and surface area on benzene adsorption capacity of activated carbons in indoor environments. Build Environ 2022;216:109011. https://doi.org/10.1016/j.buildenv.2022.109011.
[33] Raja K, Mary Jaculine M, Jose M, Verma S, Prince AAM, Ilangovan K, et al. Sol-gel synthesis and characterization of α-Fe2O3 nanoparticles. Superlattices Microstruct 2015;86:306–12.
[34] Hakim A, Marliza TS, Abu Tahari MN, Yusop MR, Mohamed Hisham MW, Yarmo MA. Development of α-Fe2O3 as adsorbent and its effect on CO2 capture. Mater Sci Forum 2016;840:421–6. https://doi.org/10.4028/www.scientific.net/MSF.840.421.
[35] Li J, Shi C, Bao A. Design of boron-doped mesoporous carbon materials for multifunctional applications: dye adsorption and CO2capture. J Environ Chem Eng 2021;9(3):105250.
[36] Posadas E, Szpak D, Lombó F, Domínguez A, Díaz I, Blanco S, et al. Feasibility study of biogas upgrading coupled with nutrient removal from anaerobic effluents using microalgae-based processes. J Appl Phycol 2016;28(4):2147–57.
[37] Meier L, Stará D, Bartacek J, Jeison D. Removal of H2S by a continuous microalgae-based photosynthetic biogas upgrading process. Process Saf Environ Prot 2018;119:65–8. https://doi.org/10.1016/J.PSEP.2018.07.014.
[38] Lei C, Zhang L, Yang K, Zhu L, Lin D. Toxicity of iron-based nanoparticles to green algae: effects of particle size, crystal phase, oxidation state and environmental aging *. Environ Pollut 2016;218:505–12. https://doi.org/10.1016/j.envpol.2016.07.030.
[39] Rana MS, Prajapati SK. Resolving the dilemma of iron bioavailability to microalgae for commercial sustenance. Algal Res 2021;59:102458. https://doi.org/10.1016/j.algal.2021.102458.
[40] Pádrová K, Lukavský J, Nedbalová L, Čejková A, Cajthaml T, Sigler K, et al. Trace concentrations of iron nanoparticles cause overproduction of biomass and lipids during cultivation of cyanobacteria and microalgae. J Appl Phycol 2015;27(4):1443–51.
[41] Rana MS, Bhushan S, Sudhakar DR, Prajapati SK. Effect of iron oxide nanoparticles on growth and biofuel potential of *Chlorella* spp. Algal Res 2020;49:101942. https://doi.org/10.1016/j.algal.2020.101942.
[42] Marchello AE, Barreto DM, Lombardi AT. Effects of titanium dioxide nanoparticles in different metabolic pathways in the freshwater microalga *Chlorella sorokiniana* (Trebouxiophyceae). Water Air Soil Pollut 2018:229. https://doi.org/10.1007/s11270-018-3705-5.
[43] Romero N, Visentini FF, Márquez VE, Santiago LG, Castro GR, Gagneten AM. Physiological and morphological responses of green microalgae *Chlorella vulgaris* to silver nanoparticles. Environ Res 2020:189. https://doi.org/10.1016/j.envres.2020.109857.
[44] Kadar E, Rooks P, Lakey C, White DA. The effect of engineered iron nanoparticles on growth and metabolic status of marine microalgae cultures. Sci Total Environ 2012;439:8–17. https://doi.org/10.1016/j.scitotenv.2012.09.010.
[45] Cheng J, Zhu Y, Li K, Lu H, Shi Z. Calcinated MIL-100(Fe) as a CO2 adsorbent to promote biomass productivity of *Arthrospira platensis* cells. Sci Total Environ 2020:699. https://doi.org/10.1016/j.scitotenv.2019.134375.
[46] Vargas-Estrada L, Longoria A, Arias DM, Okoye PU, Sebastian PJ. Role of nanoparticles on microalgal cultivation: a review. Fuel 2020:280. https://doi.org/10.1016/j.fuel.2020.118598.
[47] Dinc SK, Vural OA, Kayhan FE, San Keskin NO. Facile biogenic selenium nanoparticle synthesis, characterization and effects on oxidative stress generated by UV in microalgae. Particuology 2022;70:30–42. https://doi.org/10.1016/j.partic.2021.12.005.
[48] Bibi M, Zhu X, Munir M, Angelidaki I. Bioavailability and effect of α-Fe2O3 nanoparticles on growth, fatty acid composition and morphological indices of *Chlorella vulgaris*. Chemosphere 2021;282:131044. https://doi.org/10.1016/j.chemosphere.2021.131044.
[49] Shokri A, Fard MS. A critical review in Fenton-like approach for the removal of pollutants in the aqueous environment. Environ Challenges 2022;7:100534. https://doi.org/10.1016/j.envc.2022.100534.